Structure and Orientation of Sarcolipin in Lipid Environments[†,‡]

Alessandro Mascioni,[§] Christine Karim,[||] George Barany,[§] David D. Thomas,[||] and Gianluigi Veglia*[,§]

Department of Chemistry and Department of Biochemistry, Molecular Biology, and Biophysics, University of Minnesota, Minneapolis, Minnesota 55455

Received June 15, 2001; Revised Manuscript Received October 4, 2001

ABSTRACT: Sarcolipin (SLN) is a 31 amino acid integral membrane protein that regulates Ca-ATPase activity in skeletal muscle. Here, we report the three-dimensional structure and topology of synthetic SLN in lipid environments, as determined by solution and solid-state NMR spectroscopy. 2D solution NMR experiments were performed on SLN solubilized in sodium dodecyl sulfate (SDS) micelles. We found that SLN adopts a highly defined α-helical conformation from F9 through R27, with a backbone RMSD of 0.65 Å and a side chain RMSD of 1.66 Å. The N-terminus (M1 through L8) and the C-terminus (S28 through Y31) are mostly unstructured. The orientation of the SLN was determined using one-dimensional ^{15}N NMR solid-state spectroscopy. The protein was incorporated into phospholipid bilayers prepared from a mixture of 1,2-dioleoyl-*sn*-glycero-3-phosphocholine and 1,2-dioleoyl-*sn*-glycero-3-phosphoethanolamine. The ^{15}N chemical shift solid-state spectra from selectively labeled SLN samples indicate that SLN orients perpendicularly to the plane of the membrane bilayers. These results support the proposed mechanism of Ca-ATPase regulation of SLN via protein−protein intramembranous interactions between the highly conserved transmembrane domains of the Ca-ATPase and the conserved transmembrane domain of SLN.

Muscle contraction is initiated by the release of calcium from the sarcoplasmic reticulum (SR), which pumps Ca^{2+} ions actively into its lumen by means of the Ca-ATPase or sarco(endo)plasmic reticulum calcium pump (SERCA).[1] Three separate genes encode the SERCA family: SERCA1, SERCA2, and SERCA3. SERCA1 is exclusively expressed in fast-twitch skeletal muscle. During development, the SERCA1 gene undergoes splicing to form SERCA1a, the adult isoform, and SERCA1b, a neonatal isoform. For SERCA2, four different transcripts have been found. The most studied isoform, SERCA2a, is characteristic of slow-twitch, cardiac, and smooth muscle. Finally, SERCA3 expression is limited to lymphoid cells, platelets, mast cells, and the epithelial and endothelial cells of various organs. SERCAs are highly conserved 110 kDa integral membrane proteins, belonging to the P-type ATPase family, that couple ATP hydrolysis to calcium transport. Recently, the structure of SERCA1a has been solved at 2.4 Å resolution, revealing many interesting features of this complex enzyme but leaving the details of its regulation mechanisms unexplained (*1*).

SERCA function has been widely studied (*2*), particularly with respect to the enzymatic activity of both SERCA1a and SERCA2a. The most accepted mechanistic model includes a transition of the enzyme between two conformations: E1 with high Ca^{2+} affinity, and E2 with low Ca^{2+} affinity (*2*). According to this model, enzyme phosphorylation and MgATP binding drive calcium translocation, and the regulation mechanism relies on small transmembrane proteins that co-purify with SERCAs (*2*). Failures in this mechanism lead to imbalances in calcium homeostasis, causing severe diseases such as muscle myopathies (*3*), and toxic response to anesthetics (*4*). For instance, a loss of SERCA1a function is involved in the exercise-induced impairment and relaxation of skeletal muscle in Brody's disease, and abnormal SERCA2a regulation mechanism is involved in the progression of dilated cardiomyopathy (*3*).

SLN is a 31 amino acid integral membrane protein that co-purifies with SERCA1 (*5*−*7*). SLN has been shown to regulate the Ca-ATPase in the sarcoplasmic reticulum of skeletal muscle (*6*, *7*). Like phospholamban (PLB), the cardiac muscle regulator (*5*), SLN inhibits Ca-ATPase at low Ca^{2+} concentration. However, in contrast to PLB, SLN also activates the Ca-ATPase at high Ca^{2+} concentration and does

[†] This work was supported in part by grants to G.V. University of Minnesota (Graduate School) Structural Biology Program), D.D.T. (NIH GM27906; University of Minnesota Academic Health Center), C.K. (AHA 9930083N), and G.B. (NIH GM51628).

[‡] The coordinates for all sarcolipin conformers have been deposited in the PDB database (http://www.rcsb.org/pdb/index.html) under PDB ID code 1JDM.

* Author to whom correspondence should be addressed at the Department of Chemistry, University of Minnesota, 207 Pleasant St. S.E., Minneapolis, MN 55455. Telephone: (612) 625-0758. Fax: (612) 626-7541. E-mail: veglia@chem.umn.edu.

[§] Department of Chemistry.

[||] Department of Biochemistry, Molecular Biology, and Biophysics.

[1] Abbreviations: Ca-ATPase, calcium ATPase; COSY-DQF, correlated spectroscopy double quantum filtered; DOPC, 1,2-dioleoyl-*sn*-glycero-3-phosphocholine; DOPE, 1,2-dioleoyl-*sn*-glycero-3-phosphoethanolamine; SLN-FC, C-terminus flagged sarcolipin; HPLC, high-pressure liquid chromatography; HSQC, heteronuclear single quantum coherence; MALDI-TOF, matrix-assisted laser desorption/ionization time-of-flight; MgATP, magnesium/ATP complex; NADH, nicotinamide adenine dinucleotide; NMR, nuclear magnetic resonance; NOESY, nuclear Overhauser effect spectroscopy; PLB, phospholamban; SLN, sarcolipin; RMSD, root-mean-square deviation; SDS, sodium dodecyl sulfate; SERCA, sarco(endo)plasmic reticulum calcium pump; TAD, torsion angle dynamics; TFA, trifluoroacetic acid; TFE, trifluoroethanol; TM, transmembrane; TOCSY, total correlation spectroscopy; TSPA, 3-(trimethylsilyl)propionic acid.

10.1021/bi011243m CCC: $22.00
Published on Web 12/14/2001

not appear to be a phosphorylation substrate; instead, SLN's regulation of the Ca-ATPase probably occurs through its variable expression (*8*). SLN and PLB both have a highly conserved transmembrane domain (*7*). Since several of the 10 transmembrane helices in all SERCA isoforms are also highly conserved, the conservation of the single transmembrane domain in both PLB and SLN suggests that both interact in a similar way with Ca-ATPase. The structural similarity between the *sln* and the *plb* genes, and the homology in their protein sequences, has led Odermatt et al. to propose that the two genes are members of a family (*6*, *7*).

In this paper, we report the high-resolution structure of SLN in SDS micelles and its orientation in lipid bilayers, as determined by solution and solid-state NMR methods, respectively. This represents the first step in characterizing the complex interactions between SLN and the Ca-pump at an atomic level.

EXPERIMENTAL PROCEDURES

Peptide Synthesis. SLN and its "flag" derivative, SLN-FC (SLN-M_{32}DYKDDDDK$_{40}$), were prepared by following stepwise Fmoc solid-phase peptide synthesis and HPLC purification protocols similar to those described previously for phospholamban (*9*). Starting with Fmoc-Tyr(tBu)-PAC-PEG-PS resin (0.75 g, loading 0.16 mmol/g), the 31 residue SLN was assembled on a Milligen 9050 automated peptide synthesizer. Acidolyzable side-chain protecting groups were 2,2,5,7,8-pentamethylchroman-6-sulfonyl (Pmc) for arginine, N^{ω}-triphenylmethyl (Trt) for asparagine and glutamine, *tert*-butyl ester (O*t*Bu) for glutamic acid, and *tert*-butyl ethers (*t*Bu) for serine, threonine, and tyrosine. Fmoc removal was achieved with 20% piperidine and 2% DBU in NMP (6 min from G30 to L25; 10 min from L24 to L10; 13 min from Phe 9 to Met 1). HBTU/HOBt/DIEA couplings (4 equiv each over resin-bound amine) involved 7 min of preactivation time and the following reaction times: 1 h from G30 to L25; 1 + 0.5 h (double coupling) from L24 to L10; 2 + 0.5 h (double coupling) from F9 to M1. To deprotect and cleave the peptide from the resin (200 mg each time), first an Fmoc removal step was carried out, followed by treatment with 2 mL of freshly prepared Reagent R: 90% TFA, 5% thioanisole, 3% 1,2-ethanedithiol, 2% anisole, for 4 h at 25 °C. The cleavage mixture was filtered, and the resin was washed with 2 mL of the same cocktail. The combined filtrates were concentrated under N_2, and 30 mL of diethyl ether was added at 0 °C. The precipitated peptide was collected by centrifugation, and washed 3 times with 30 mL of cold diethyl ether. The crude peptide was dissolved in 5 mL of TFA and purified by HPLC on a Diphenyl column (Vydac, 219TP152022; 15−20 μm, 300 Å; 22 × 250 mm) that had been equilibrated with 95% water, 2% acetonitrile, 3% 2-propanol. Peptide elution was achieved with a linear gradient to a final solvent composition of 5% water, 38% acetonitrile, 57% 2-propanol (*10*). Fractions containing peptides were lyophilized to yield 12 mg of SLN (10% yield based on 200 mg of peptide-resin). For syntheses of selectively labeled ^{15}N derivatives of SLN, ^{15}N-labeled Fmoc amino acids were used as obtained from Cambridge Isotope Laboratories (Andover, MA). The composition of each peptide was verified by amino acid analysis, and its molecular mass was verified by matrix-assisted laser desorption/ionization time-of-flight (MALDI-TOF) mass spectrometry. SLN showed a peak at 3761.20 *m*/*z*, [M+H], which corresponded to the calculated molecular mass of 3761.63 Da. Mass spectral analysis of SLN with ^{15}N-labels at L8, L21, and L24 showed an *m*/*z* value of 3764.21, [M+H].

The synthesis of SLN with the "flag" at the C terminus started with Fmoc-Lys(Boc)-PAC-PEG-PS resin (0.75 g, loading 0.186 mmol/g). Additional acidolyzable side-chain protecting groups were *tert*-butyloxycarbonyl (*t*Boc) for lysine, *tert*-butyl esters (O*t*Boc) for aspartic acid, and *tert*-butyl ethers (*t*Bu) for tyrosine. The SLN flag residues M_{32}-DYKDDDDK$_{40}$ were manually assembled by checking each coupling and deprotection step with the ninhydrin test. Fmoc removal was achieved with 20% piperidine and 2% DBU in NMP (10 min from D40 to D36; 30 min from K35 to M32). HBTU/HOBt/DIEA (4 equiv each over resin-bound amine) couplings from D39 to D36 involved 1 h reaction time. HATU/HOAt/DIEA (4 equiv) couplings were used for K35 and Y34, with a reaction time of 1 + 1 h (double coupling), and for D33 and M32, HBTU/HOBt/DIEA (4 equiv) couplings with 1 h reaction time. From Y31 on, the 40 residue SLN-FC was assembled on a Milligen 9050 automated peptide synthesizer as already described. Deprotection, cleavage, and HPLC purification in the same way provided 9.5 mg of SLN-FC (5% yield based on 200 mg of peptide-resin).

Functional Assays. The functional assay consisted of two steps: (a) co-reconstitution of Ca-ATPase with SLN and (b) measurement of Ca-ATPase activity, essentially as described previously for PLB (*10*, *11*). For the co-reconstitution, SLN (33 μg) was dried and dissolved in a 4:1 solution of 1,2-dioleoyl-*sn*-glycero-3-phosphocholine (DOPC)/1,2-dioleoyl-*sn*-glycero-3-phosphoethanolamine (DOPE) in chloroform (total amount of lipid 2.4 mg). After eliminating the organic solvent by N_2 flux, the lipid/SLN mixture was suspended in imidazole buffer at pH 7 and sonicated to form vesicles, which were added to a solution of Ca-ATPase in detergent (octyl glucoside). The detergent was then eliminated from the preparation by using Biobeads SM2 (Cal Biochem, San Diego, CA) for 3 h at room temperature. A control sample was prepared by the same procedure, with the omission of the SLN. For the functional assay, a portion of the vesicle mixture containing 60 μg of Ca-ATPase, with or without the desired amount of SLN, was added to a 200 μL incubation solution containing 0.5 mM phosphoenol pyruvate, 2.5 mM ATP, 0.2 mM NADH, 2 IU of pyruvate kinase, 2 IU of lactate dehydrogenase, and 1−2 μg of calcium ionophore (A23187). The rate of ATP hydrolysis was measured from the rate of decrease in NADH absorbance at 340 nm, using a microplate spectrophotometer (Thermomax, Molecular Devices).

Solution NMR Spectroscopy. The NMR samples were prepared by dissolving ~0.7 mg of the lyophilized SLN in 500 μL of 20 mM aqueous sodium phosphate (pH 6.5), and 600 mM perdeuterated sodium dodecyl sulfate (SDS-d_{25}) containing 10% ^2H_2O. The pH of the sample was ~4.0 from a direct uncorrected pH-meter reading. All NMR spectra were recorded using a Varian Unity spectrometer operating at 800 MHz at a temperature of 50 °C. An inverse detection triple-resonance probe was used. Resonance assignments were performed using two-dimensional ^{1}H/^{1}H TOCSY (40−70 ms mixing times) and ^{1}H/^{1}H NOESY (100, 150, 200 ms

mixing time) experiments (*12*). Water suppression was achieved using the WATERGATE technique (*13*). Spectra were collected with 256 complex points in the t_1 dimension and 1024 data points in the t_2 dimension. TOCSY spectra were acquired using DIPSY2 pulse sequence (*14*, *15*). The spectral widths were 9 kHz on both t_1 and t_2 dimensions. Proton chemical shifts were referenced to internal 3-(trimethylsilyl)propionic acid (TSPA). To simplify the assignment of crowded regions of the NOESY spectra, two specifically labeled samples of SLN were prepared (G2 and L16 ^{15}N-labeled SLN and L8, L21, L24 ^{15}N-labeled SLN). To determine the intraresidue connectivities on these samples, 2D NOESY−HSQC spectra were run with a mixing time of 100 ms. NMR spectra were processed using NMRPipe (*16*) and analyzed using SPARKY (*17*). 2D spectra were processed with a 90° shifted sine bell window function. The data were zero-filled to twice the size before Fourier transformation. In the 100 ms NOESY spectrum, NOE cross-peaks were integrated and used for the structure calculations. The NOE volumes were calibrated using the average NOE volume from resolved aromatic vicinal protons and from the amide−amide cross-peaks in the helical region. The NOE volumes were classified as strong, medium, and weak, corresponding to distance restraints of 1.9−2.7, 1.9−3.3, and 1.9−5.0 Å, respectively (*18* and references cited therein).

The solvent accessibility of the amide backbone signals was determined by proton deuterium exchange studies. These experiments were carried out by dissolving the protonated protein sample containing SDS-d_{25} in ^2H_2O and subsequently monitoring the disappearance of the NH peaks by 1D and 2D NMR. Analysis of the 1D data after 30 min at 50 °C showed a general reduction in the amide envelope intensity, but the presence of several amide peaks. Since these peaks could not be identified using the 1D spectrum, we used 2D NOESY data to determine the slowly exchanging amide peaks. The peaks indicated in the NMR summary (Figure 2) with a filled dot do not exchange significantly over a period of 3 days of incubation at 50 °C, and were used as constraints in the structure calculations.

Structure Calculations. Structure calculations were performed using CNS (*19*), starting from extended structures (*20*), and using a combination of torsion angle dynamics (TAD) (*21*) and Cartesian dynamics. An initial TAD (high temperature) phase consisting of 1000 molecular dynamics steps each of 15 fs was performed at a temperature of 50 000 K. During this stage, all of the force constants were kept constant. Subsequently, a Cartesian dynamics cooling phase comprised of 20 000 steps each of 15 fs was employed with the temperature decreasing from 1000 to 0 K during this interval. Finally, a second cooling phase (12 000 steps with a 5 fs time step, starting from a temperature of 2000 K) was employed using Cartesian dynamics with parameters starting from their values during the high-temperature TAD phase and increasing to their final values over the duration of this interval. A total of 264 NOEs were used in the calculations, of which 163 were intraresidue and 101 interresidue NOEs. A total of 15 hydrogen bond constraints were incorporated at the end of our preliminary calculations, and 15 Hα chemical shift restraints were used for the final refinement of the structures. Fifty structures were generated, and the 16 lowest energy structures were selected for analysis. The analysis of the structures and the NOE violations was carried out with the "accept.inp" routine included in the CNS software package. The 16 structures showed no violations of (a) NOE constraints higher than 0.3 Å, (b) bond angles higher than 5°, and (c) bond lengths higher than 0.05 Å. The covalent geometry of the conformers generated was determined using PROCHECK_NMR (*22*).

Solid-State NMR Spectroscopy. For the preparation of the vesicles, a lipid mixture of 44 mg of a 4:1 ratio of DOPC and DOPE in $CHCl_3$ was dried at room temperature using a stream of N_2. The lipids were suspended uniformly in 10 mL of distilled, deionized water. The suspension was sonicated using a Branson Sonifier model 450 at lower power with a microtip. Sonication was stopped when the suspension became transparent (∼30 min). A solution of 1−2 mg of SLN in 500 μL of 20 mM phosphate buffer and 600 mM SDS at pH ∼4 was prepared separately and mixed with the vesicles. The mixture was diluted with 10 mL of distilled, deionized water, frozen in liquid N_2, and thawed at room temperature. The detergent was eliminated by extensive dialysis against water at room temperature (∼2 days). The mixture was spread in a thin layer onto twenty 10 × 8 × 0.1 mm glass plates. After drying in an oven/incubator at a temperature of 42 °C, the plates were stacked together and placed in a sealed chamber along with saturated aqueous $NH_4H_2PO_4$ (∼93% relative humidity). The chamber was incubated at 42 °C for 12−14 h. The final sample was wrapped in Parafilm and placed in a plastic bag to stabilize hydration. The sample was then placed in the flat coil probe with the plane of the glass plates and the membrane bilayers perpendicular to the direction of the applied magnetic field. Alternatively, the samples were made by preparing DOPC/DOPE 4:1 mixture in 5 mL of chloroform and by evaporating the solvent with a stream of N_2. The protein (typically 1−2 mg) dissolved in 100 μL of TFE was added to the lipid preparation. The mixture was spread onto ∼20 glass plates and dried under vacuum for 12 h. The plates with the lipids and the protein were hydrated in the 42 °C chamber already described.

All solid-state NMR spectra were acquired using a Chemagnetics CMX-400 MHz spectrometer operating at 400.1 MHz for ^{1}H and equipped with a flat-coil double-resonance ^{1}H/^{15}N probe with coil dimensions of 10 × 10 × 5 mm (Doty Scientific). The samples were cooled with a stream of air at 25 °C. To determine the orientation of the phospholipids on the glass plates, one-dimensional ^{31}P spectra were acquired using single-pulse excitation with ^{1}H decoupling during acquisition (*23*−*25*). The ^{15}N one-dimensional spectra were acquired using the cross-polarization pulse sequence (*26*). The typical spin-lock time used was 1 ms, the recycle delay 10 s, and the spin-lock field about 40 kHz. The spectra were processed using an exponential apodization function corresponding to a line broadening of 200 Hz before Fourier transformation. Chemical shifts were referenced with respect to $(NH_4)_2SO_4$ (27 ppm).

RESULTS

Solution NMR. As with other membrane proteins, sample preparation is a crucial step in obtaining high-resolution spectra of SLN in detergent micelles (*27*). Although SLN does not have a tendency to form specific oligomers in detergents, it tends to form large aggregates in the range of concentrations (1−2 mM) suitable for NMR studies (*10*).

The spectroscopy was optimized by preparing different samples containing different peptide:detergent ratios, with the best conditions found to be ~0.7 mM SLN in 600 mM SDS. Higher concentrations of peptide caused severe broadening of the resonances and a loss in NMR spectra sensitivity (data not shown). While temperature played an important role in sample optimization, pH changes in a range from 4 to 6.5 did not significantly affect proton line shape. The optimal temperature for obtaining high-resolution spectra of SLN was found to be 50 °C. Under these conditions, the samples were stable for months, as determined by the reproducibility of 1D and 2D NMR spectra.

Due to the slow reorientation of the SLN/micelle complexes, TOCSY spectra show only few amide/Hα correlations, complicating the assignment process. These interruptions in the "sequential walk" are very common in membrane protein spectra (Veglia et al., unpublished results). To overcome this difficulty and to obtain full assignment of the backbone and side chain resonances, we synthesized different ^{15}N selectively labeled SLN samples. Two different SLN samples were prepared, one with a G2 and L16 ^{15}N-labeled SLN, and the other with L8, L21, and L24 ^{15}N-labeled SLN. These samples were used to run NOESY−HSQC at short mixing times (20−40 ms) to identify the amide/Hα correlations for those amino acids whose resonances fall into the most crowded region of the NOESY spectrum. The aliphatic and aromatic regions were assigned by using both NOESY spectra at relatively short mixing times and TOCSY spectra of the protein dissolved in 100% ^2H_2O. All of the resonance assignments are reported in the Supporting Information. Due to the broad lines of the amide resonances, we could not derive useful information or dihedral angle constraints from the DQF-COSY spectra. A portion of the 2D NOESY spectrum at 300 ms is reported in Figure 1, illustrating the amino acid residue assignments using cross-peaks between a backbone amide proton and the α-proton of the preceding residue.

A summary of the NOE cross-peak pattern between the backbone amide and the Hα and Hβ protons is provided in Figure 2. Given the resolution of our spectra, very few ambiguities are present in the NOE assignments; those are indicated in gray. One problem was the most mobile region of the N-terminus, which displayed a lower population of NOEs. The region between F9 and R27 shows a very dense population of NOEs, but it was possible to identify most of the dαN(i, i+1), dNN(i, i+1), and dβN(i, i+1) correlations. This region also shows a remarkable number of dαβ(i, i+3) and dαN(i, i+3), typical of regular α-helices. Only two dαN(i, i+4) correlations were detected, one between I14 and V18, and the other between M22 and V26. The most significant amide−amide peaks are reported in Figure 1B. A plot with the total number of NOEs per residue, including both backbone and side chains, is shown in Figure 3A. The α-helical conformation is also supported by the Hα chemical shifts (Figure 2). The analysis of the hydrogen bonds was carried out by 2D NOESY spectroscopy. We observed very slow exchange in the helical region of SLN. The protonated protein was first lyophilized and then resolubilized in 100% ^2H_2O and incubated for ~4 days at a temperature of 50 °C. Most of the peaks corresponding to the helical region were still present and were used in the structure calculations. The resonances of the solvent-exposed amides of the two termini disappeared after 10 min.

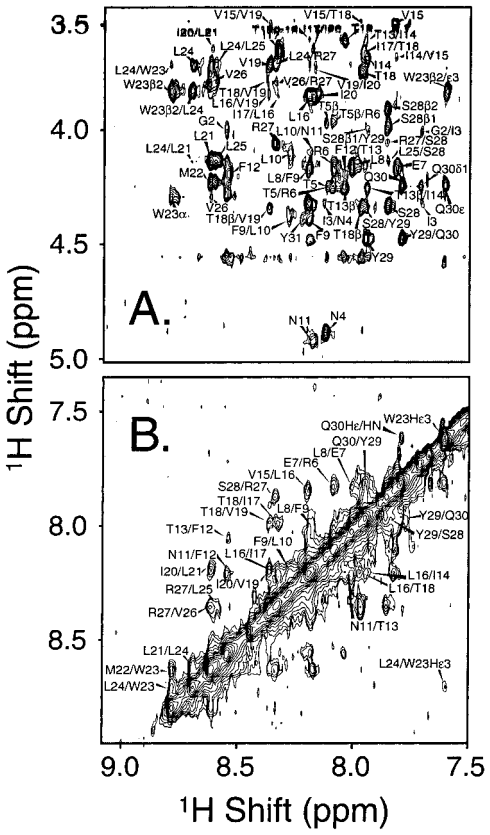

FIGURE 1: Selected regions of the ^{1}H/^{1}H NOESY spectrum of SLN in detergent micelles at 100 ms mixing time: (A) fingerprint region, (B) amide region.

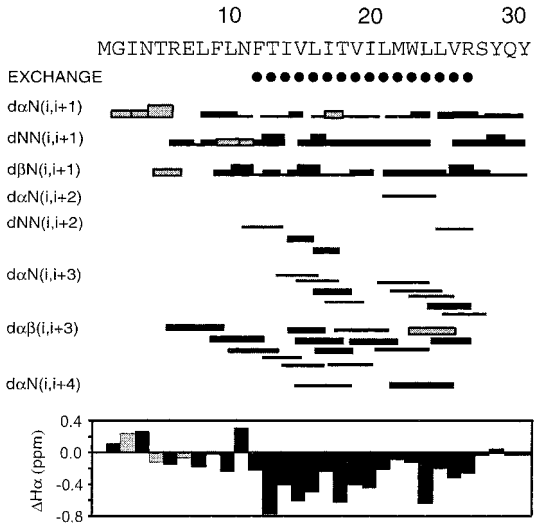

FIGURE 2: Summary of NMR structural parameters of SLN in SDS micelles. The correlations indicated with gray correspond to the ambiguous assignments due to resonance overlapping.

The superposition of the 16 best structures from the simulated annealing calculations is reported in Figure 4. The ensemble of the low-energy conformers has a backbone RMSD of ~0.65 Å. The conformers generated have a well-defined structure that is predominantly α-helical (from residues 9−27). Residues 1 through 8, which constitute the small cytoplasmic domain, are mainly disordered. Only sequential NOEs were observed in that region of the protein. The C-terminus, which is proposed to be more involved in Ca-pump regulation (*6*, *7*), is more structured, although

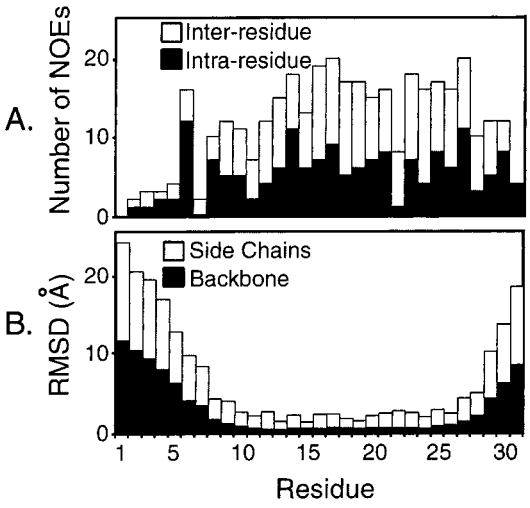

FIGURE 3: (A) Histogram picturing the number of intra- and interresidue NOEs as a function of the residue. (B) RMSD of backbone and side chains for the 16 lowest energy conformers derived from simulated annealing calculations.

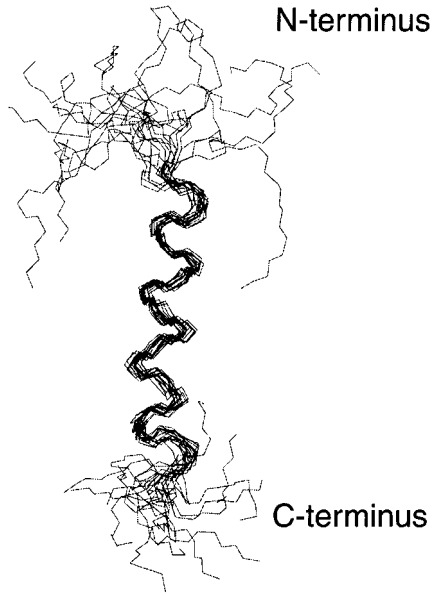

FIGURE 4: Superposition of the 16 lowest energy structures of SLN. The superposition was done by fitting the backbone Cα atoms from residue 9 to residue 27.

residues Y29, Q30, and Y31 do not present a defined structure. The most hydrophilic residues are located at the N-terminus. These residues are in random conformation and are characterized by a fast exchange of the amide sites with the bulk solvent, as determined by $^{1}H/^{2}H$ exchange. The substantial number of NOEs found in the helical region (see Figure 3A) results in a resolution for the side chains of 1.66 Å for the superposition of the Cα atoms from residues 9−27. All of the statistics for the structure calculations are summarized in Table 1.

In general, the structure of SLN resembles the typical "building block" of membrane proteins: all of the residues in the transmembrane domain of the protein are hydrophobic (L, I, V), with the exception of T13 and T18; the aromatic residues (F, Y, and W) reside in the region near the lipid carbonyls; positively charged residues (R6 and R27) extend into the lipid phosphate region (*28*).

Table 1: Experimental NMR Restraints and Structural Statistics for the 16 Lowest Energy Conformers[a]

NOE	
total	264
intraresidue	163
interresidue	101
hydrogen bonds	15
average energies (kcal mol^{-1})	
E_{tot}	156 ± 28
E_{NOE}	42 ± 9
E_{bond}	8 ± 1
E_{angle}	55 ± 10
$E_{improper}$	6 ± 1
E_{VDW}	44 ± 10
restraint violations	
>0.5 Å	0
RMSD (Å)	
superposition Cα 9−27	0.65
Ramachandran analysis (residues 9−27)[a] (%)	
residues in most favored regions	81.9
residues in additional allowed regions	18.1
residues in generously allowed regions	0
residues in disallowed regions	0

[a] All the statistics were carried out using CNS. Ramachandran analysis was carried out using PROCHECK_NMR (*22*).

SLN-FC Structure. We also carried out NMR experiments on SLN-FC (SLN-M_{32}DYKDDDDK$_{40}$), which is reported to have a "super-inhibitory" effect (*6*). From the superposition of the TOCSY and NOESY experiments carried out on the wild-type and SLN-FC mutant, we observe the same NOE and chemical shift patterns for residues 9 through 27, indicating that they have the same conformation in that region. While residues 29 through 31undergo substantial changes in their chemical shifts, no changes in their intraresidue NOE patterns were observed. The flag, constituted of eight charged amino acids, gives a unique envelope of resonances centered at 7.8 ppm, showing that this flag is unstructured.

Solid-State NMR. The orientation of SLN in lipid bilayers was evaluated by ^{15}N solid-state NMR spectra in mechanically oriented samples (*27*, *29*−*32*). For SLN, we used two different protein sample preparation methods (see Experimental Procedures) that yielded identical results for the samples analyzed. Our first step was to establish the macroscopic orientation of the lipid bilayers using one-dimensional ^{31}P spectroscopy (*23*−*25*). Figure 5 shows one-dimensional ^{31}P spectra of a vesicle preparation (Figure 5A) and mechanically oriented lipid bilayers (Figure 5B), both with DOPC:DOPE in a ratio of 4:1. The chemical shift of ^{31}P is a function of the orientation of the tensor. This vesicle preparation results in the typical chemical shift of the isotropic ^{31}P spectrum. The oriented ^{31}P sample has a peak at about 30 ppm. Once the orientation of the lipid bilayers was established, we carried out one-dimensional ^{15}N spectroscopy. Figure 6 shows the one-dimensional solid-state ^{15}N NMR spectra of specifically ^{15}N-labeled SLN in lipid bilayers; Figure 6A shows the unoriented spectrum of SLN ^{15}N specifically labeled at residue 21; Figure 6B shows the oriented spectrum of SLN ^{15}N specifically labeled at positions 2 and 16; and Figure 6C shows the oriented spectrum of SLN ^{15}N specifically labeled at positions 8, 21, and 24.

The magnitudes and orientations of ^{15}N chemical shift tensors have been reported for model peptides (*33*−*37*). Reference values for the magnitudes of the principal elements

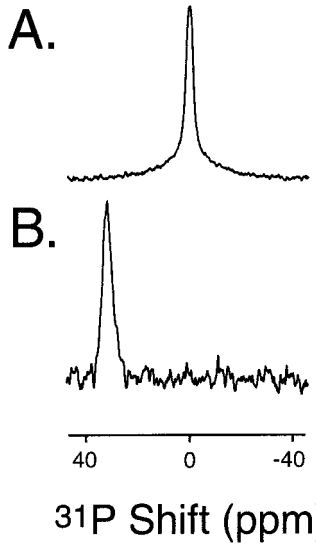

FIGURE 5: One-dimensional ^{31}P NMR spectra of DOPC/DOPE vesicles (A) and DOPC/DOPE lipid bilayers on glass plates. The spectra were referenced to phosphoric acid (0 ppm).

were reported to be $\sigma_{11} = 64$ ppm, $\sigma_{22} = 77$ ppm, and $\sigma_{33} = 217$ ppm for parallel, isotropic, and perpendicular orientation of the NH tensor with regard to the membrane bilayer plane (*37*), respectively. We have assigned the two ^{15}N resonances according to the high-resolution structure of SLN obtained in SDS micelles. L16, which is located in the middle of the α-helical region, can be assigned to the resonance at ∼203 ppm, indicating a perpendicular orientation of the NH tensor with respect to the membrane bilayer. On the other hand, the resonance at about 90 ppm can be attributed to G2, which is located outside the bilayer (Figure 6B). This finding is in agreement with the high-resolution structure in micelles. The unoriented spectrum of the SLN ^{15}N selectively labeled at position 21 shows the typical powder pattern spectrum (Figure 6A) (*38*). The second sample analyzed was the L8, L21, and L24 specifically^{15}N-labeled SLN (Figure 6C). We obtained only one unique peak located in the left side of the spectrum centered at ∼188 ppm, indicating that the three leucine residues lay perpendicularly to the plane of the bilayer.

Although we would need additional NMR frequency data to completely assign the structure of SLN in lipid bilayers (*39*, *40*), the information obtained from these initial one-dimensional solid-state NMR studies shows that the overall orientation of SLN is perpendicular to the plane of the membrane bilayers.

DISCUSSION

While inhibitory and structural effects of PLB on the Ca-ATPase are relieved by phosphorylation (*41*), the mechanisms of control by SLN are still totally unknown. In fact, SLN possesses neither phosphorylation sites nor glycosylation or acetylation sites (*5*, *6*). One recent hypothesis is that the regulatory function of SLN in SERCA1 might be modulated over the long term by the level of SLN expression rather than by SLN phosphorylation (*8*).

There are striking similarities between PLB and SLN, which share a remarkable homology in the TM region (*7*). In a recent study, the biochemical properties of SLN were analyzed and compared to those of the homologous region

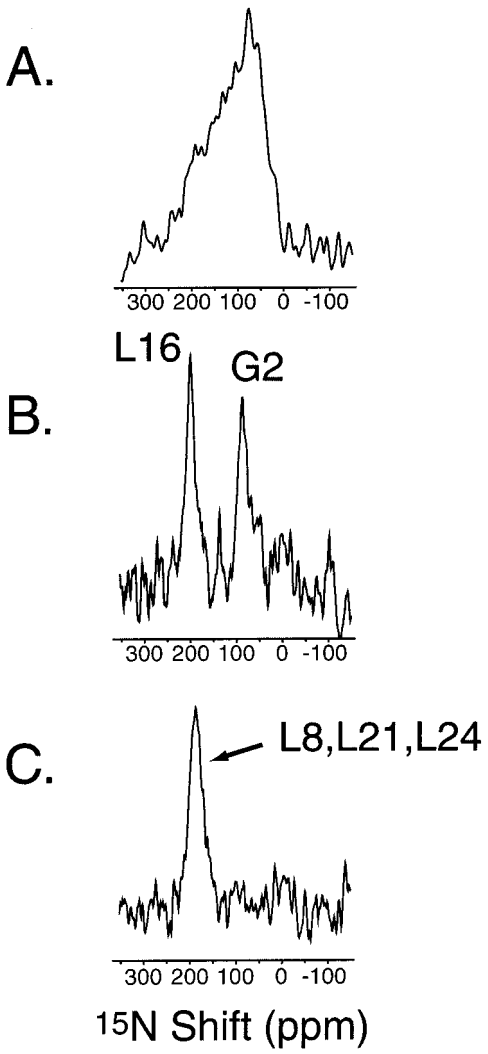

FIGURE 6: One-dimensional solid-state ^{15}N NMR spectra of specifically ^{15}N-labeled SLN in lipid bilayers: (A) powder pattern spectrum of L21 ^{15}N-labeled SLN in lipids; (B) oriented spectrum of G2L16 ^{15}N-labeled SLN in lipid bilayers; (C) oriented spectrum of L8L21L24 ^{15}N-labeled SLN in lipid bilayers. The ^{15}N spectra were referenced to ^{15}N-labeled $(NH_4)_2SO_4$ (70 ppm).

of PLB (PLB_{26-52}) (*10*). Despite the high homology of the TM domains, it was found that SLN has a much lower tendency to form oligomers. The self-association of SLN also occurs only at very high concentrations, while the PLB_{26-52} fragment has a very pronounced tendency to form pentamers at very low concentrations. The functional reconstitution of Ca-ATPase with SLN and PLB_{26-52}, respectively, showed that both proteins regulate the Ca-ATPase by inhibiting the enzyme at low (submicromolar) Ca^{2+} concentrations and activating the Ca-ATPase at high Ca^{2+} concentrations. Although PLB_{26-52} and SLN have the same effect on the Ca-ATPase, full-length PLB and SLN differ substantially in their regulation mechanisms. While PLB reduces calcium affinity at low Ca^{2+} concentrations, it does not have any effect at higher concentrations. SLN, on the other hand, has a lower inhibitory effect at low Ca^{2+} concentrations, but acts on the V_{max} (activity at saturating calcium) of the enzyme, increasing it by 30−40% (*6*, *10*). A comparison of different protein regulatory activities on Ca-ATPase is reported in Figure 7. Note that all four regulatory proteins represented in the graph inhibit the activity at low Ca^{2+} concentration

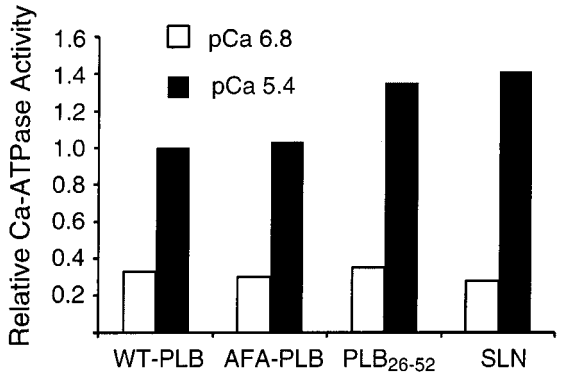

FIGURE 7: Effect of regulatory proteins on Ca-ATPase activity, showing the activity measured in the presence of the regulatory protein divided by the activity in its absence [3.65 μmol of P_i released (mg of Ca-ATPase)$^{-1}$ min^{-1}], adapted from reference (*12*). As described previously (*10*, *11*), Ca-ATPase was reconstituted in lipid bilayers (DOPC:DOPE 4:1 ratio, 40 mg of lipid/mg of Ca-ATPase) with and without 10 mol of regulatory protein/mol of Ca-ATPase, and the Ca-ATPase activity was measured at 25 °C. Values given are the mean of 3 measurements, with standard deviations less than 10% of the observed values. ATPase values are reported at low [Ca^{2+}] (pCa 6.8) and at saturating [Ca^{2+}] (pCa 5.4). WT-PLB is the 52 residue wild-type phospholamban, which is primarily pentameric. AFA-PLB is the PLB mutant C36A,C41F,C46A, which is predominantly monomeric. PLB_{26-52} is the isolated transmembrane domain of PLB. Note that all four regulatory proteins inhibit the Ca-ATPase at low [Ca], while PLB_{26-52} and SLN also activate at high [Ca].

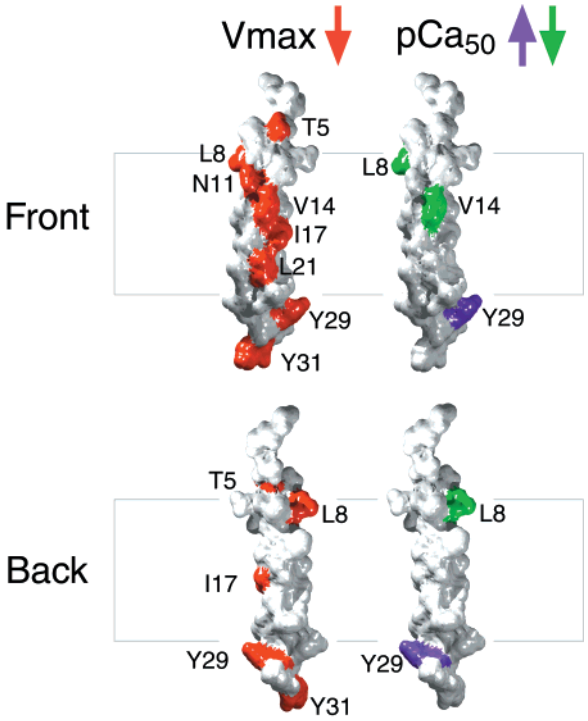

FIGURE 8: Map of the SLN amino acids affecting the functional interaction with SERCA1, according to Odermatt et al. (*6*). Residues in red represent a decrease of V_{max} upon mutation of wild-type residues to alanine. Residues in purple and green represent an increase and a decrease of pCa values, respectively, upon mutation of wild-type residues to alanine.

(pCa 6.8), while PLB_{26-52} and SLN also activate Ca-ATPase at saturating calcium concentration (pCa 5.4). This functional similarity suggests that structural analysis of SLN will provide insight into the relationship between structure and function in PLB. This is important, because the present study of SLN represents the first high-resolution structure in a lipid environment of any of the family of proteins that regulate the Ca-ATPase.

While there is still no direct physical evidence that defines the structural interactions between the calcium pump and these two modulators (SLN and PLB), functional studies of PLB carried out by MacLennan and co-workers have helped identify the specific sites that might be responsible for the inhibitory effect (*42*−*44*). These extensive site-directed mutagenesis studies have led to the hypothesis that a small cluster of amino acids located in the transmembrane 6 (TM6) domain of the calcium pump is crucial for PLB inhibition, and concluded that the hydrophobic face of PLB interacts with TM6, while the more hydrophilic face may interact with TM4 (*44*). In the high-resolution structure of Ca-ATPase (E1 form with high-calcium affinity), both TM6 and TM4 are buried in the core of the transmembrane domain of the pump. The key residues of the cluster identified by MacLennan are F809, T805, L802, and V795, which all face the lipid bilayer in the high-resolution structure of SERCA1a (*1*). The most exposed residue is F809, which is located at the lipid bilayer interface. Using a similar approach, MacLennan and co-workers identified the functional "hot-spots" in the intramembrane interaction between the SERCA1a and SLN (*6*). They ruled out phosphorylation as the regulation mechanism for SLN activity and concluded that the N-terminal sequence is not critical for the interaction with the Ca pump. In fact, these researchers found that the addition of a flag sequence to the N-terminus (M_1DYKDDDDK$_9$-SLN) does not modify protein activity, while the addition of a flag to the C-terminus (SLN-M_{32}DYKDDDDK$_{40}$) generates a "super-inhibitor" mutant.

Our structural analysis of the latter mutant shows that the flag domain is unstructured. Further structural analysis of the SLN-FC mutant in its functional complex with the Ca pump is needed to determine whether the flag domain assumes a specific inhibitory structure.

Other mutations from the wild-type sequence of the SLN transmembrane domain to alanines or glutamic acid have different effects on the Ca-ATPase inhibitory activity. We have summarized these different effects in Figure 8, using a surface representation of the high-resolution structure that we have determined. Reading the mutagenesis results in light of the high-resolution structure, we see that most of the residues affecting the protein activity are located on the same face of SLN. Although a complete functional alanine scan of SLN has not yet been completed, this finding supports MacLennan's hypothesis of a preferential orientation in the interaction between SLN and Ca-ATPase, and, taken together with the functional results on SLN and PLB_{26-52} (Figure 7), shows that the interactions of the Ca-ATPase with PLB and SLN occur with similar mechanisms via intramembranous interactions (*10*).

Thus, the high-resolution structure of SLN contributes to our understanding of the complex interactions between SLN and Ca-ATPase. It should now be possible to design different mutants to "fine-tune" the activity of SLN and to test these mutants in in vitro and in vivo experiments to determine the structural bases of the calcium regulation mechanism in skeletal and cardiac muscle (*45*).

CONCLUSION

We report here the high-resolution structure of SLN in lipid environments. As determined by a combination of 2D solution and ^{15}N one-dimensional solid-state NMR spectroscopy, SLN possesses a compact α-helical transmembrane domain (from residue 9 through residue 27), which is oriented perpendicularly to the plane of the membrane. The N-terminus, which does not have functional relevance, is mobile in both micelles and lipid bilayers. We have also analyzed the structure of SLN-FC, which is reported to have super-inhibitory activity. We found that this mutant has the same structure as native SLN in its most conserved region, while the added "flag" at the C-terminus is totally unstructured. These studies constitute the first steps toward characterization of intramembrane interactions between SLN and Ca-ATPase.

ACKNOWLEDGMENT

We thank Z. Zhang for assistance in synthesizing and purifying the peptide, R. Di Fonzo, M. Mesleh, and D. Jones for helpful comments, and D. Live and B. Ostrowski for assisting with the NMR experiments, T. Krick and Dr. L. A. Higgins for assistance in the Facility for Mass Spectrometry in the Life Sciences at the University of Minnesota, and J. Johnson and Dr. L. Dangott for assistance in amino acid analysis at the Protein Chemistry Laboratory, Texas A&M University. We benefited from the outstanding facilities at the Minnesota High-Field NMR Center in the Department of Biochemistry, Molecular Biology, and Biophysics; and the Solid State NMR facility in the Department of Chemistry, University of Minnesota. NMR instrumentation was provided with funds from the NSF (BIR-961477) and the University of Minnesota Medical School.

SUPPORTING INFORMATION AVAILABLE

Table showing resonance assignments of ^{15}N selectively labeled SLN samples (3 pages). This material is available free of charge via the Internet at http://pubs.acs.org.

REFERENCES

1. Toyoshima, C., Nakasako, M., Nomura, H., and Ogawa, H. (2000) *Nature 405*, 647−655.
2. Stokes, D. L., and Wagenknecht, T. (2000) *Eur. J. Biochem. 267*, 5274−5279.
3. MacLennan, D. H. (2000) *Eur. J. Biochem. 267*, 5291−5297.
4. Karon, B. S., Geddis, L. M., Kutchai, H., and Thomas, D. D. (1995) *Biophys. J. 68*, 936−945.
5. Wawrzynow, A., Theibert, J. L., Murphy, C., Jona, I., Martonosi, A., and Collins, J. H. (1992) *Arch. Biochem. Biophys. 298*, 620−623.
6. Odermatt, A., Becker, S., Khanna, V. K., Kurzydlowski, K., Leisner, E., Pette, D., and MacLennan, D. (1998) *J. Biol. Chem. 273*, 12360−12369.
7. Odermatt, A., Taschner, P. E. M., Scherer, S. W., Beatty, B., Khanna, V. K., Cornblath, D. R., Chaudhry, V., Yee, W. C., Schrank, B., Karpati, G., Breuning, M. H., Knoers, N., and MacLennan, D. H. (1997) *Genomics 45*, 541−553.
8. Gayan-Ramirez, G., Vanzeir, L., Wuytack, F., and Decramer, M. (2000) *J. Physiol. 524*, 387−397.
9. Karim, C. B., Stamm, J. D., Karim, J., Jones, L. R., and Thomas, D. D. (1998) *Biochemistry 37*, 12074−12081.
10. Hellstern, S., Pegoraro, S., Karim, C. B., Lustig, A., Thomas, D. D., Moroder, L., and Engel, J. (2001) *J. Biol. Chem. 276*, 30845−30852.
11. Karim, C. B., Marquardt, C. G., Stamm, J. D., Barany, G., and Thomas, D. D. (2000) *Biochemistry 39*, 10892−10897.
12. Kumar, A., Ernst, R. R., and Wuthrich, K. (1980) *Biochem. Biophys. Res. Commun. 95*, 1−6.
13. Piotto, M., Saudek, V., and Skelnar, V. (1992) *J. Biomol. NMR 2*, 661−665.
14. Bax, A., and Davis, D. G. (1985) *J. Magn. Reson. 65*, 355−360.
15. Shaka, A. J., Lee, C. J., and Pines, A. (1988) *J. Magn. Reson. 77*, 274−293.
16. Delaglio, F., Grzesiek, S., Vuister, G. W., Zhu, G., Pfeifer, J., and Bax, A. (1995) *J. Biomol. NMR 6*, 277−293.
17. Goddard, T. D., and Kneller, D. G. *SPARKY 3*, University of California, San Francisco, 1999.
18. Roberts, G. C. K. (1993) *NMR Macromol.* 333−353.
19. Brünger, A. T., Adams, P. D., Clore, G. M., DeLano, W. L., Gros, P., Grosse-Kunstleve, R. W., Jiang J., Kuszewski, J., Nilges, M., Pannu, N. S., Read, R. J., Rice, L. M., Simonson, T. and Warren, G. L. (1998) *Acta Crystallog., Sect. D 54*, 905−921.
20. Nilges, M., Gronenborn, A. M., Brünger, A. T., and Clore, G. M. (1988) *Protein Eng. 2*, 27−38.
21. Stein, E. G., Rice, L. M., and Brünger, A. T. (1997) *J. Magn. Reson. 124*, 154−164.
22. Laskowski, R. A., Rullman, J. A. C., MacArthur, M. W., Kaptein, R., and Thornton, J. M. (1998) *J. Biomol. NMR 8*, 477−486.
23. Seelig, J. (1977) *Q. Rev. Biophys. 10*, 353−418.
24. Seelig, J. (1978) *Biochim. Biophys. Acta 515*, 105−140.
25. Seelig, J., Macdonald, P. M., and Scherer, S. W. (1987) *Biochemistry 26*, 7535−7541.
26. Pines, A. M., Gibby, M. G., and Waugh, J. S. (1973) *J. Chem. Phys. 59*, 569−590.
27. Opella, J. (1997) *Nat. Struct. Biol. 4*, 845−848.
28. von Heijne, G. (1999) *Q. Rev. Biophys. 32*, 285−307.
29. Cross, T. A., and Opella, S. J. (1994) *Curr. Opin. Struct. Biol. 4*, 574−581.
30. Marassi, F., and Opella, S. J. (1998) *Curr. Opin. Struct. Biol. 8*, 640−648.
31. Kovacs, F. A., and Cross, T. A. (1997) *Biophys. J. 73*, 2511−2517.
32. Kim, Y., Valentine, K., Opella, S. J., Schendel, S. L., and Cramer, W. A. (1998) *Protein Sci. 7*, 342−348.
33. Harbison, G. S., Jelinsky, L. W., Stark, R. E., Torchia, D. A., Herzfeld, J., and Griffin, R. G. (1984) *J. Magn. Reson. 60*, 79−82.
34. Hartzell, C. J., Whitfield, M., Oas, T. G., and Drobny, G. P. (1987) *J. Am. Chem. Soc. 109*, 5966−5969.
35. Oas, T. G., Hartzell, C. J., Dahlquist, W., and Drobny, G. P. (1987) *J. Am. Chem. Soc. 109*, 5962−5966.
36. Teng, Q., and Cross, T. A. (1989) *J. Magn. Reson. 85*, 439−447.
37. Wu, C., Ramamoorthy, A., Gierasch, L. M., and Opella, S. J. (1995) *J. Am. Chem. Soc. 117*, 6148−6149.
38. Opella, S. J. (1985) *Q. Rev. Biophys. 131*, 327−361.
39. Ketchem, R. R., Hu, W., and Cross, T. A. (1993) *Science 261*, 1457−1460.
40. Opella, S. J., Marassi, F. M., Gesell, J. J., Valente, A. P., Oblatt-Montal, M., and Montal, M. (1998) *Nat. Struct. Biol. 6*, 375−379.
41. Thomas, D. D., Reddy, L. G., Karim, C. B., Li, M., Cornea, R., and Stamm, J. (1998) *Ann. N.Y. Acad. Sci. 853*, 186−195.
42. Rice, W. J., Green, N. M., and MacLennan, D. H. (1997) *J. Biol. Chem. 272*, 31412−31419.
43. Rice, W. J., and MacLennan, D. H. (1996) *J. Biol. Chem. 271*, 31412−31419.
44. MacLennan, D. H., Kimura, Y., and Toyofuku, T. (1998) *Ann. N.Y. Acad. Sci. 853*, 31−42.
45. Kiriazis, H., and Kranias, E. G. (2000) *Annu. Rev. Physiol. 62*, 321−351.

BI011243M